Journal of Interfaces, Thin films, and Low dimensional systems 5 (2) Winter and Spring (2022) 505-515

Modeling a high-performance broadband mid-infrared modulator using graphene-based hybrid plasmonic waveguide

Scientific research paper

Mohammad Reza Jafari[1*], Akbar Asadi[2]

[1]*Department of Condensed Matter Physics, Faculty of Physics, Alzahra University, Tehran, Iran*

[2]*Department of Physics, Faculty of Science, Imam Khomeini University of Maritime Science, Nowshahr, Iran*

ARTICLE INFO

Article history:
Received 27 December 2022
Revised 15 March 2023
Accepted 20 March 2023
Available online 19 April 2023

Keywords
Graphene
Plasmonic
Waveguide
Modulator
mid-infrared
Finite element method

ABSTRACT

A graphene based-hybrid plasmonic waveguide (GHPW) with unique geometric structure is designed for surface plasmon polariton guidance and modulation at the frequency area of 10 to 30 THz. The GHPW is consist of a graphene layer in the middle, a high-density polyethylene (HDPE) gating layer, and two interior dielectric delimiter layers and two exterior semi-cylinder Germanium substrates symmetrically embedded on both edges of the graphene. Because of the matchless semi-cylinder structure design, the electromagnetic wave interaction with graphene ultimate subwavelength SPPs strong confinement with long propagation length. Small normalized mode area of $\sim 10^{-4}$ and long propagation length of 10.67-28.92 μm at Fermi energy of 1.0 eV is attained for SPPs modes propagation of the GHPW in the frequency bound of 10-30 THz and semi-cylinder radius R > 450 nm, respectively. By controlling the graphene Fermi energy, it is found that the structure has a modulation depth higher than 20 % for the frequency band of 10-30 THz and arrives at the peak of approximately 100 % at the frequency greater than 28.75 THz. To benefit from the great broadband MIR propagation and modulation efficiency, the GHPW may promise different MIR waveguides, modulators, photonic, and optoelectronic devices.

1 Introduction

Mid-infrared (MIR), an electromagnetic radiation (EMR) with the frequency band of 6-100 THz, has attracted much attention due to their phenomenal utilizations in spectroscopy [1], communications [2], imaging [3], sensing [4], modulation [5], absorbing [6,7] etc. Waveguides guide the electromagnetic waves with less loss of energy and are utilized as ingredients in optical integrated circuits or as optical communication systems. It would be considered promising to expand novel MIR waveguides with premier features of strong confinement, less loss, and plasticity tunability. The coupling between an incident wave and the plural oscillation of electrons at the interface between a metal and a dielectric generates surface Plasmon polaritons (SPPs) [8-11]. The dielectric-based waveguides include silicon-on-glass waveguides [12], photonic crystal fibers [13], and slab waveguides [14]. Compared to these waveguides, the metal-based hybrid plasmonic waveguides (MHPW) are mighty of guiding electromagnetic wave with subwavelength confinement *smaller* than the *diffraction limit*, indicating excellent ability in highly integrated optical circuits [15,16]. Recently, in order to enhance the SPPs propagation distance, various

*Corresponding author.
Email address: Mo.jafari@alzahra.ac.ir
DOI: 10.22051/jitl.2023.42299.1077

types of MHPW as wedged, channeled, and metal gap plasmonic waveguides have been studied [17-19]. It is detected that the SPPs guided by MHPW can attain the normalized mode area of $\sim 10^{-3} - 1$ and long propagation length of $\sim 0.01 - 100$ mm at the wavelength of 1.55 μm. Nevertheless, immediately expanding the waveguide design to the MIR spectrum will direct to a considerable decay in the subwavelength confinement, making it inappropriate for compact integration [20]. Therefore, by utilizing the dielectric materials without electrostatic adjustability, like noble metals, all forenamed waveguides suffer from the intrinsic defect not tunable once the waveguides are fixed after construction.

Graphene, as a monolayer of carbon atoms, has absorbed a number of researchers owing to its unique electrical, optical, and mechanical properties [21,22]. Graphene is attended to as one of the Excellent plasmonic materials to replace metals with comparatively great field confinement, long propagation length, exclusively with important preference of being strongly tunable through chemical doping or electrostatic doping, due to supporting surface plasmon polaritons in the infrared spectrum [23,24].

The graphene plasmonic waveguides represent field confinement with the wavelength two orders less than that in free space [25-28]. The graphene adjustable attributes through electrostatic doping without altering the device dielectric materials and geometric configuration, enable the graphene with a vast potential application in different tunable infrared systems. In recent years, many graphene-based plasmonic devices (GPDs) such as absorbers [29], sensing [30,31], biosensors [32], switches [33], modulators [5,34], and waveguides [35-38] have been investigated.

In this regard, for example, L Ye et al. [5] investigated a GHPW for MIR propagation and modulation in the frequency area of 10 to 20 THz. They have displayed their proposed waveguide which can attain excellent SPPs propagation performance with propagation length of 12.1μm-16.7μm, attenuation of 0.28-0.36 dB/μm, and transmission of 92-94% in the frequency area of 10 to 20 THz with the graphene Fermi energy of 1.0 eV [5].

In the present research, we design a unique GHPW for propagation and modulation of extremely broadband MIR surface plasmon polaritons. The proposed unique structure has schemed of a graphene layer in the middle, a high-density polyethylene (HDPE) gating layer, two interior dielectric buffer layers, and two exterior semi-cylinder Germanium substrates symmetrically embedded on both edges of the graphene. Firstly, we model the SPPs mode distributions, propagation distance, effective refractive index, normalized mode area, and figure of merit of the hybrid plasmonic waveguide. The designed waveguide can attain excellent SPPs propagation efficiency with propagation length of 11-29μm, attenuation of 0.21-0.4 dB/μm, and transmission of 91-96% in the frequency range of 10 to 30 THz at the graphene Fermi energy of 1.0 eV.

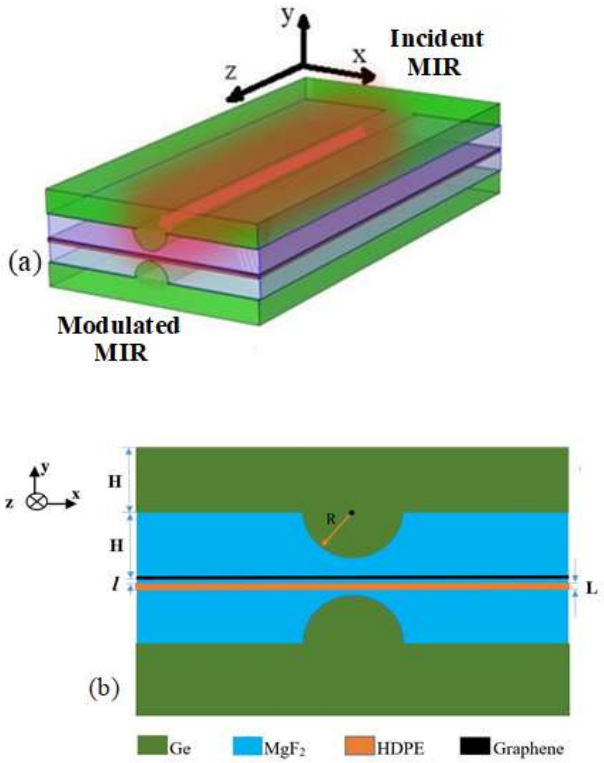

Figure 1. (a) Three-dimensional structure of the proposed waveguide GHPW. (b) cross-section of the waveguide.

Hence, the designed structure supports higher figure of merit, longer propagation distance and lower attenuation compared to similar plasmonic waveguides (e.g., see [5]). This research prepares a new path to modeling GHPW for extremely effective broadband MIR propagation and modulation and may propose some exciting solutions for MIR devices.

2 Design and techniques

The structure of the proposed novel GHPW is indicated in Fig. 1, which is composed of two equal exterior semi-cylindrical substrates and two similar interior delimiter layers located on both edges of graphene in the waveguide middle. The substrate layers are supposed to be germanium (Ge) with height H=600 nm and the relative permittivity $\varepsilon_{Ge} = 16.2$. Also, the delimiter layers are presumed to be magnesium fluoride (MgF_2) with height H=600 nm and the relative permittivity $\varepsilon_{MgF_2} = 1.7$ [39–41]. The dual germanium semi-cylinder, with their radius as R=370 nm, expand into the MgF_2 layers to amplify interaction of electromagnetic wave to graphene and SPPs confinement. A high-density polyethylene (HDPE) slab with the relative permittivity $\varepsilon_{HDPE} = 2.37$ [42] and height $L = 20$ nm are embedded within the lower MgF_2 layer with thickness l=10 nm underneath the graphene for gating design. The gate voltage is exerted to the graphene and HDPE layer to tune the Fermi energy of graphene, as demonstrated in Fig. 1(a).

In this paper, we apply the finite element technique for modeling and analyzing the features of the designed GHPW. The graphene light features are described by a surface conductivity σ_g, which can be computed via the Kubo Integral formulation with the interband and intraband conductivity terms [5]

$$\sigma_g(\omega, E_F, \tau, T) = \sigma_{intra}(\omega, E_F, \tau, T) + \sigma_{inter}(\omega, E_F, \tau, T), \quad (1)$$

$$\sigma_{intra}(\omega, E_F, \tau, T) = \frac{je^2}{\pi\hbar^2(\omega - j/\tau)} \int_0^{\infty} \left(\frac{\partial f_d(\xi, E_F, T)}{\partial \xi} - \frac{\partial f_d(-\xi, E_F, T)}{\partial \xi} \right) \xi d\xi, \quad (2)$$

$$\sigma_{inter}(\omega, E_F, \tau, T) = \frac{-je^2\left(\omega - \frac{j}{\tau}\right)}{\pi\hbar^2} \times \int_0^{\infty} \left(\frac{f_d(-\xi, E_F, T) - f_d(\xi, E_F, T)}{(\omega - j/\tau)^2 - 4(\frac{\xi}{\hbar})^2} \right) d\xi, \quad (3)$$

and

$$f_d(\xi, E_F, T) = \{\exp[(\xi - E_F)/k_B T] + 1\}^{-1}, \quad (4)$$

where E_F is the chemical potential or Fermi energy, it can be set from 0.0 to 1.0 eV through the gating structures [43-45]. Also, quantities of ω, $\tau = \mu E_F / e v_F^2$, T, e, ξ, $\hbar = h/2\pi$, k_B and $f_d(\xi, E_F, T)$ are the angular frequency, the relaxation time, the temperature, the electron charge, energy, the reduced Plank constant, the Boltzmann constant, and the Fermi-Dirac distribution function, respectively. Here, it can be supposed that the temperature T = 300 K, the Fermi velocity $v_F = 10^6$ m/s and the graphene relaxation time $\tau = 1.2$ ps are obtained via the graphene carrier mobility μ [46-49]. The graphene dielectric function can be measured as in [35],

$$\varepsilon_g = 1 + i\sigma_g \eta_0 / k_0 \Delta, \quad (5)$$

where η_0 refers to air impedance, k_0 is the wavenumber, and Δ= 1 nm shows the d layer graphene thickness. These are the key plasmonic parameters that can be calculated through the changes in physical dimensions and materials. The loss tangent function is defined as [5],

$$\tan\delta = |\sigma_r / \sigma_i|, \quad (6)$$

where σ_i and σ_r are the imaginary and real parts of graphene surface conductivity σ_g, respectively. The index of effective refractive for the guided mode can be represented as [5],

$$n_{eff} = k/k_0, \quad (7)$$

where k_0 is the constant of propagation in free space and k is the propagation constant of the waveguide. The figure of merit (FOM) can be defined as [5]

$$FOM = n_r / n_i, \quad (8)$$

where n_i and n_r are the imaginary and real parts and imaginary part of n_{eff}, respectively. The imaginary part of n_{eff}, which is in charge of losses of propagation, explains the guided modes propagation length, which can be defined as [5]

$$L_p = 1/2k_0 n_i. \quad (9)$$

The normalized mode area is defined as follows [5]

$$A = A_m / A_0 = \frac{1}{A_0} \frac{\int_{-\infty}^{+\infty} S(x,y)\, dx\, dy}{\max[S(x,y)]}. \quad (10)$$

with

$$S(x,y)=\frac{1}{2}\mathrm{Re}\left\{\frac{d[\varepsilon_0\varepsilon_r(x,y)\omega]}{d\omega}\right\}|E(x,y)|^2 + \frac{1}{2}\mu_0|H(x,y)|^2, \quad (11)$$

where A_{m} is the effective mode area, S(x,y) is the electromagnetic energy density, and $A_0=\lambda_0^2/4$ is the diffraction-limited mode area in free space, respectively. Also λ_0 is the wavelength in free space. In the proposed GHPW, the dependence of gate voltage V_{g} on the Fermi energy E_{F} can be achieved by [5,43]

$$V_{\mathrm{g}}=\frac{2el}{\pi\varepsilon_r\varepsilon_0\hbar^2v_{\mathrm{F}}^2}\int_0^{\infty}\xi[f_{\mathrm{d}}(\xi,E_{\mathrm{F}},T) - f_{\mathrm{d}}(\xi,2E_{\mathrm{F}},T)]\,d\xi, \quad (12)$$

where $\varepsilon_{\mathrm{r}}=\varepsilon_{MgF_2}$. The attenuation a and transmission coefficients t of the proposed waveguide are defined by [35, 50]

$$a=\frac{40\pi\ \mathrm{Im}(n_{\mathrm{eff}})}{\lambda_0\ Ln10} \quad \& \quad t=10^{-a/10}, \quad (13)$$

Where the modulation depth of the proposed waveguide is described by recent relations.

3. Results and discussion

Firstly, the surface conductivity σ_{g} and the loss tangent $\tan\delta$ of graphene is considered at the MIR region. Figure 2 shows the σ_{g} components and loss $\tan\delta$ of graphene on frequency at Fermi energy $E_{\mathrm{F}}=0.2$, 0.6 and 1 eV. Figures 2(a) and 2(c) show that the real part and the absolute value of graphene surface conductivity (σ_{r} and $|\sigma_{\mathrm{g}}|$) are positive and decrease drastically by increasing frequency from 10 THz to 30 THz. Figure 2(b) also shows that

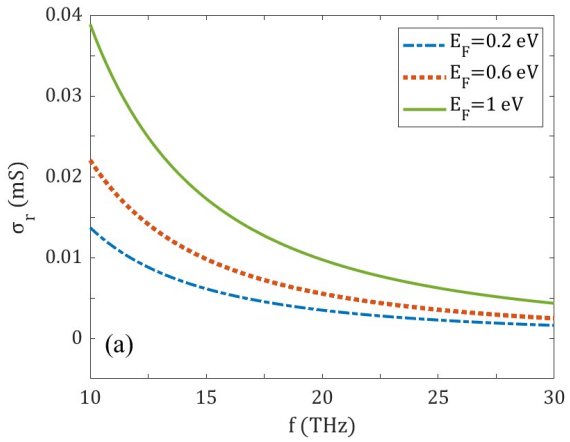

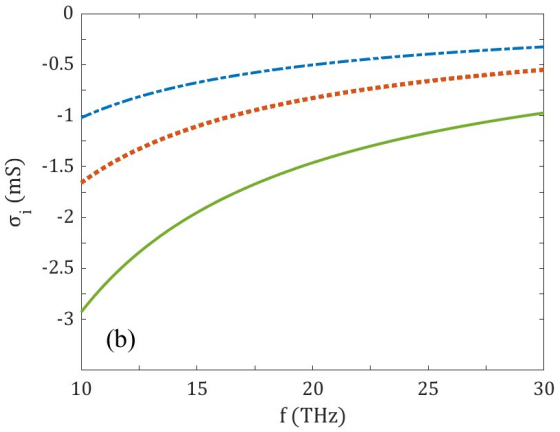

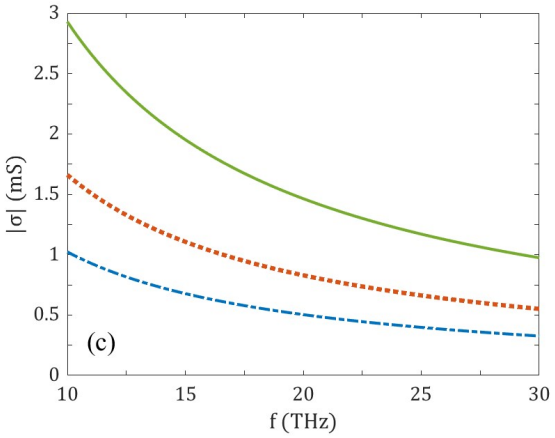

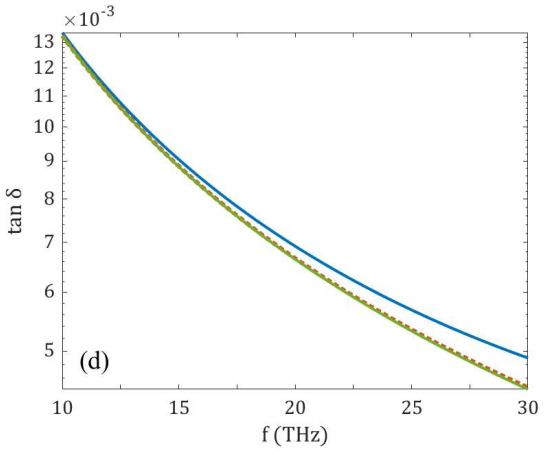

Figure 2. (a)-(d) display Dependence of the σ_{r}, the σ_{i}, the $|\sigma_{\mathrm{g}}|$ and the $\tan\delta$ of graphene respectively on frequency with Fermi energy $E_{\mathrm{F}}=0.2$, 0.6, and 1 eV.

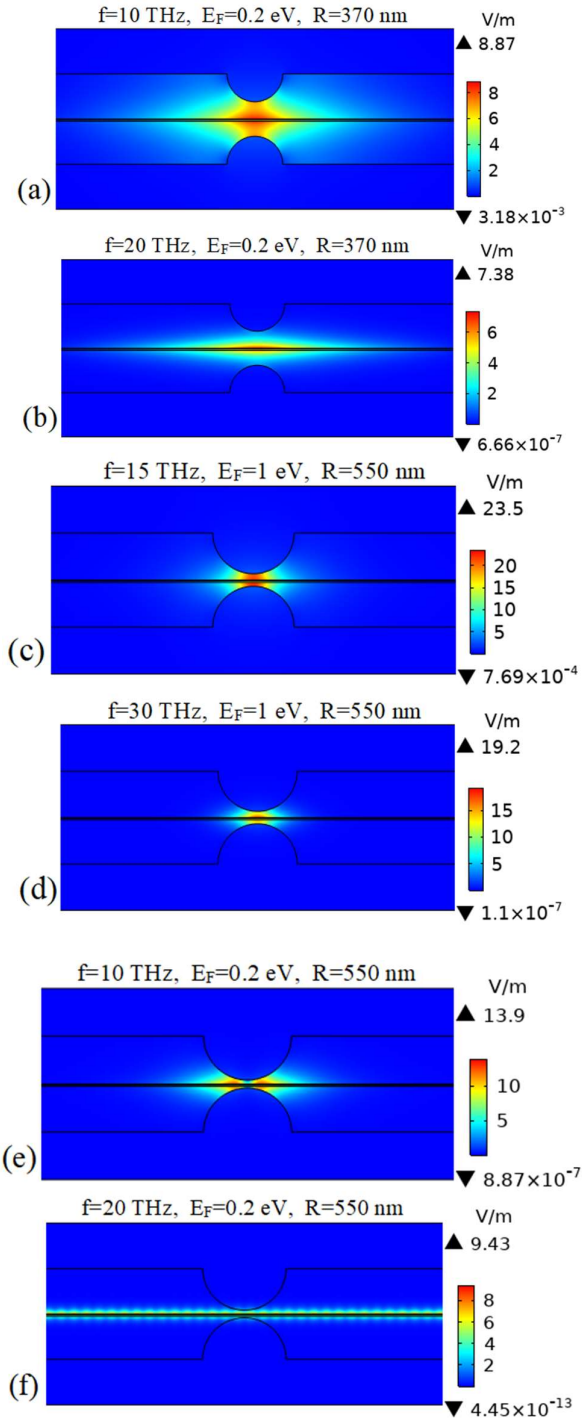

Figure 3. The distributions of electric field of the proposed structure for (a) $[f, E_F, R] = [10\ \text{THz}, 0.2\ \text{eV}, 370\ \text{nm}]$, (b) $[f, E_F, R] = [20\ \text{THz}, 0.2\ \text{eV}, 370\ \text{nm}]$, (c) $[f, E_F, R] = [15\ \text{THz}, 1\ \text{eV}, 550\ \text{nm}]$, (d) $[f, E_F, R] = [30\ \text{THz}, 1\ \text{eV}, 550\ \text{nm}]$, (e) $[f, E_F, R] = [10\ \text{THz}, 0.2\ \text{eV}, 550\ \text{nm}]$ and (f) $[f, E_F, R] = [20\ \text{THz}, 0.2\ \text{eV}, 550\ \text{nm}]$.

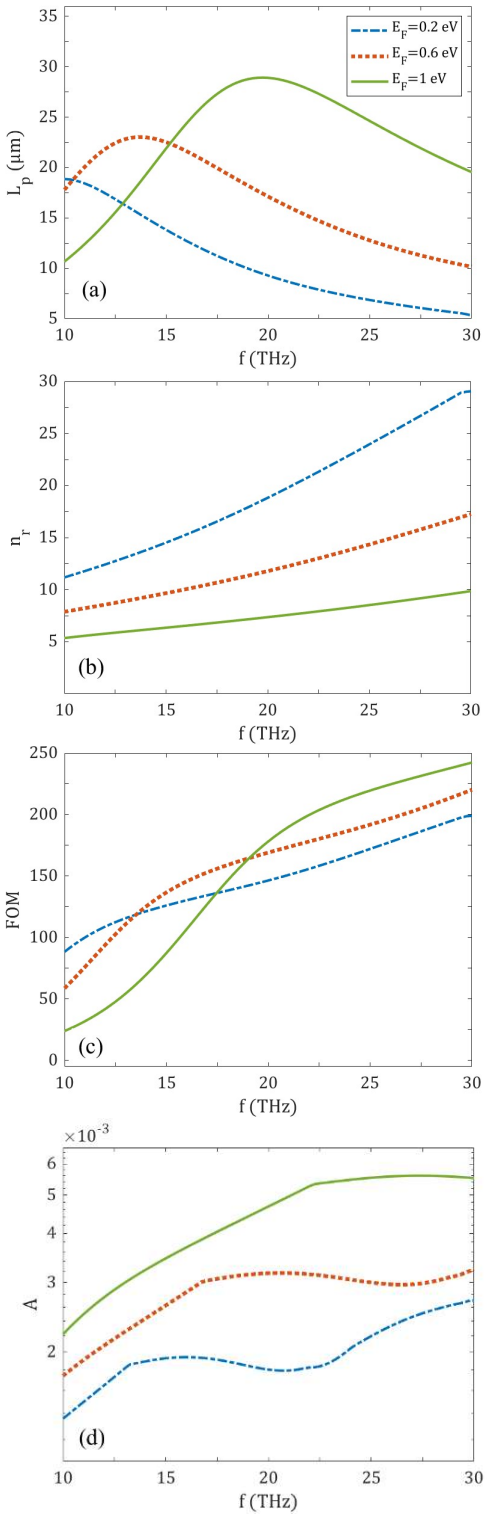

Figure 4. (a)-(d) Dependence of the L_p, the n_r, the FOM, and A on the f at different Fermi energies with R = 370 nm.

the imaginary part of the graphene surface conductivity σ_i is negative and increases by increasing frequency. Figure 2(d) demonstrates the $\tan\delta$ amounts decrease from 0.0130 to 0.0044 at both $E_F = 0.6$ and 1.0 eV, while its amount decreases from 0.0130 to 0.005 for

$E_F = 0.2$ in frequency confining from 10 THz to 30 THz.

We present the electromagnetic field distributions for the hybrid plasmonic mode with TM (transverse magnetic) for different radius R of semi-cylinder of the waveguide, frequency, and Fermi energy in Fig. 3. It can be observed that the maximum of the electric field value is distributed between double semi-cylinder around the graphene in waveguide center with R=550 nm, which its confinement is much stronger than with R=370 nm. Because of the unique structure of the waveguide, the interaction of electromagnetic waves is considerably augmented in the area between the dual semi-cylinder.

The dependence of the propagation length L_p, the real part of effective refractive index n_r, the figure of merit FOM, and the normalized mode area A on the frequency ranging from 10 to 30 THz are shown in Fig. 4 at different Fermi energies with R = 370 nm. The diagram of L_p on the frequency at $E_F = 0.6$ eV and $E_F = 1$ eV grows to their peak amounts and afterward diminishes, whereas the L_p at $E_F = 0.2$ eV diminishes contiguously. The maximum value of the propagation length is $L_p = 28.92$ nm at the frequency of $f = 19.75$ THz with $E_F = 1$ eV, which is a long propagation length compared to the proposed GHPW in reference [5], [see Fig. 4(a)]. Figure 4(b) illustrates the n_r variations of the proposed GHPW on frequency for different Fermi energies. At the fixed amount of E_F, the n_r grows when the frequency grows. While at a constant amount of the frequency, the n_r diminishes when the value of E_F grows. Figure 4(c) shows that the FOM increases as the frequency increases, implying a larger FOM is obtained at a more extensive frequency finish. Figure 4(d) shows A for the waveguide as the MIR frequency changes from 10 THz to 30 THz at different E_F. It displays that the A value of the designed structure achieves ~10^{-3}, which is sub-wavelength strong confinement of the proposed structure.

Figure 5 presents the diagram of L_p, n_r, FOM, and A on the radius R of semi-cylinder of GHPW at frequencies of 10, 20 and 30 THz with $E_F = 1$ eV. In figure 5(a), the L_p related to all three different frequencies on the radius R grows to their peak amounts and before diminishing. The maximum L_p for frequencies of 10, 30 THz are equal to 18.47 nm and 12.85 nm at R=510 nm, respectively, but the ultimate L_p for frequency of 20 THz appears at the radius R = 405 nm. Figures 5(b) and 5(c) display

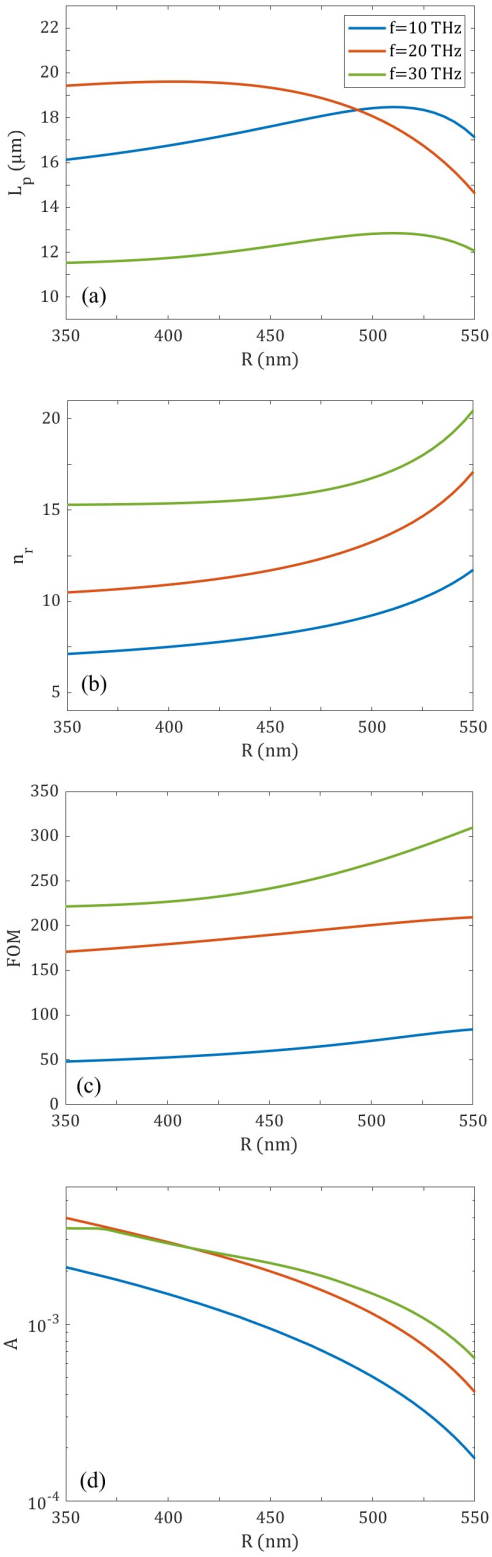

Figure 5. (a)-(d) Present the diagram of the L_p, the n_r, the FOM, and the A on the radius R of semi-cylinder of GHPW, respectively, at frequencies of 10, 20, and 30 THz with $E_F = 1$ eV.

the dependences of the n_r and FOM on the R of the semi-cylinder waveguide for different frequencies, respectively. It can be seen that the n_r and FOM decrease significantly as the frequency decreases. Fixed the frequency, the n_r, and the FOM increase with the increasing radius R. Figure 5(d) illustrates the diagram of A on the radius R semi-cylinder GHPW for different frequencies. It can be seen that when the frequency decreases, the lower A is achieved via setting the radius R of the semi-cylinder structure. It is found that at $f = 10$ THz and R=550 nm, the lowest A is decreased to 1.74×10^{-4}. Therefore, for further decrease of A to practical empirical application in modulators of nanoscale, the frequency and radius R of the semi-cylinder can be reduced.

In the following, we study the effects of the frequency, the radius R semi-cylinder of graphene-based hybrid plasmonic waveguide, and the relative permittivity of the gating layer materials on the L_p and n_r of the proposed waveguide. The comparison of L_p and n_r of the designed waveguide with various gating layer materials of aluminum oxide (Al_2O_3), silicon dioxide (SiO_2), and high-density polyethylene (HDPE) are presented in Fig. 6, where the dielectric constants of the gating layer materials are supposed as $\varepsilon_{Al_2O_3} = 8$ and $\varepsilon_{sio_2} = 3.7$ [5]. Figures 6(a) and 6(b) show the dependences of the L_p and n_r designed structure with various gating layer materials on the frequency of waveguide. Accordingly, SPPs propagation attributes may be controlled via the difference in the dielectric constant of the gating layer. Owing to the smallest dielectric constant of the HDPE, the L_p (n_r) of the designed structure with HDPE gating layer has the largest (smallest) amount with ratio to the waveguides with SiO_2 and Al_2O_3 gating layers. The dependences of the L_p and n_r GHPW structure with various gating layer materials, on radius R of the waveguide at $f = 20$ THz in Figs. 6(c) and 6(d) are shown.

Eventually, we investigate the modulation efficiency of SPPs mode for the designed waveguide. In the GHPW, the E_F can be tuned via gate voltage V_g [see Fig. 1(a)]. The dependence of V_g on E_F by Eq. (12) is shown in Fig. 7(a). It is detected that the needed amounts of V_g are about 1.84 and 44.87 V for attaining the E_F of 0.2 and 1.0 eV, respectively. Using the graphene adjustability property, the broadband SPPs modulation of the waveguide absorber may be obtained.

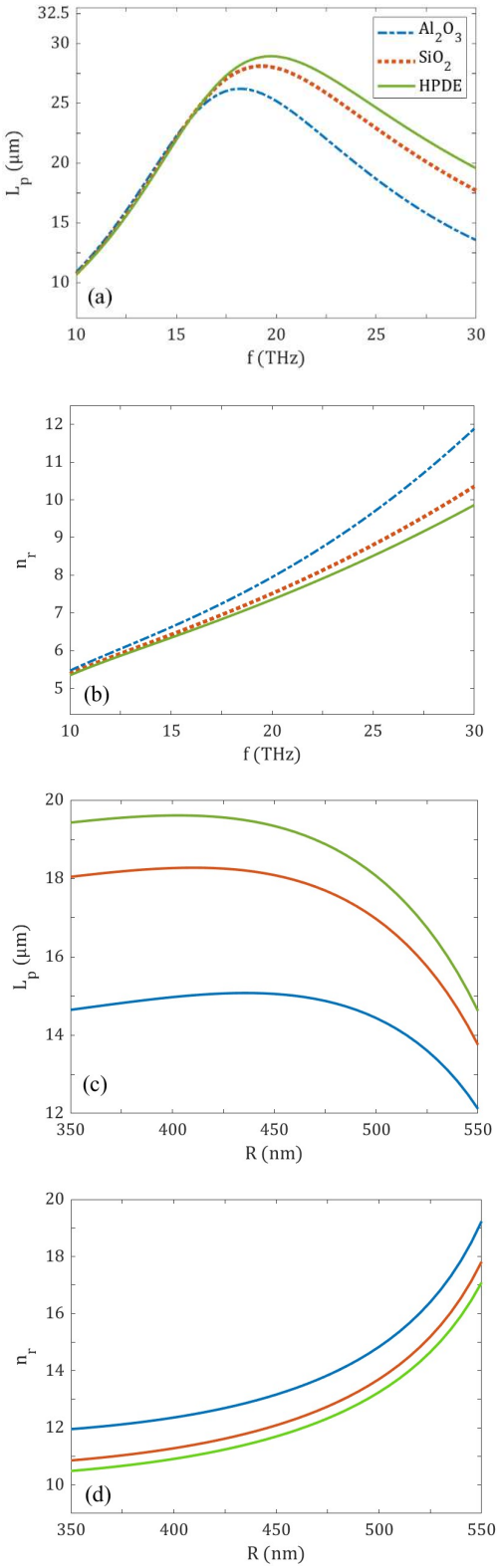

Figure 6. (a) and (b) show the dependences of the L_p and n_r designed structure with different gating layer materials, on the frequency of waveguide at R=370 nm. Also, the diagram of the L_p and n_r GHPW structure with various gating layer materials, on radius R of the waveguide at f=20 THz are exhibited in panels (c) and (d).

Furthermore, to the assessment of the modulation efficiency, the dependency of attenuation a (dB/μm) and transmission coefficient t on E_F at the frequencies 10, 20, and 30 THz are demonstrated in Figs. 7(b) and 7(c), respectively, where a and t are described with Eq. (13). It is detected that a has a considerable value at the beginning with $E_F < 0.1$ eV, and it continuously decreases with the E_F increasing at different frequencies. For example, a can be rapidly reduced from 1100 to 0.23 dB/μm, on E_F, and t is increased from 0 to 0.95 on the E_F at $f = 20$ THz. Because of the matchless waveguide configuration, greatly augmented interaction of the electromagnetic wave with graphene and subwavelength SPPs confinement in the region between the dual semi-cylinder can be attained. The attenuation modulation features of this proposed waveguide which are superordinate to the broadband waveguide modulator is reported, which has a typical attenuation modulation e.g., ranging from 3.39 dB/μm to 50.94 dB/μm on the frequency at range 10 to 30 THz with $E_F = 1$ eV [5]. Here, we tune the graphene Fermi energy from $E_F = 0.2$ eV or $V_g = 1.84$ v as the "OFF" state point to $E_F = 1.0$ eV or $V_g = 44.87$ v as the "ON" state point of the proposed structure. Also, the modulation depth is calculated with $\eta = (t_{ON} - t_{OFF})/t_{ON}$ [5, 51]. Figures 7(d) and 7(f) show the dependence of attenuation α and transmission t coefficient on frequency f in different Fermi energies, respectively. Also, Figure 7(f) shows the changes of the proposed waveguide modulation depth on frequency. It is observed that a and t change from 0.15 dB/μm to 0.41 dB/μm and 91-97% at ON state, respectively. Where both of them alter from 0.23 to 0.81 dB/μm and 95%-82% at OFF state while the frequency increase from 10 THz to 30 THz. the modulation depth notably augments with augmenting frequency f. Here, the designed structure can attain the modulation depth higher than 20% among 10 and 30 THz and reach a peak of 100% at $f > 28.75$ THz.

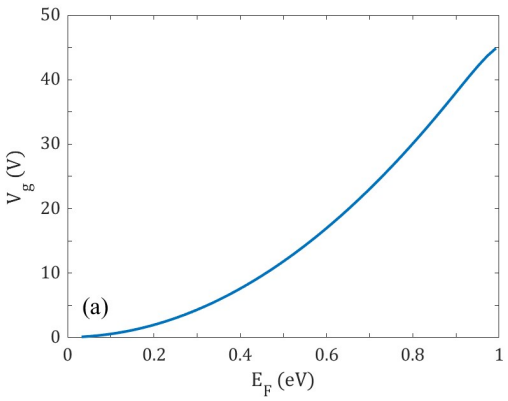

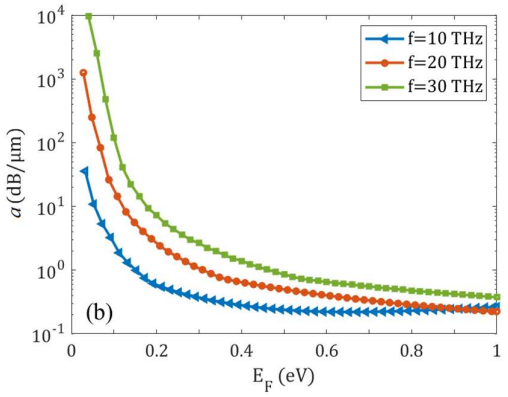

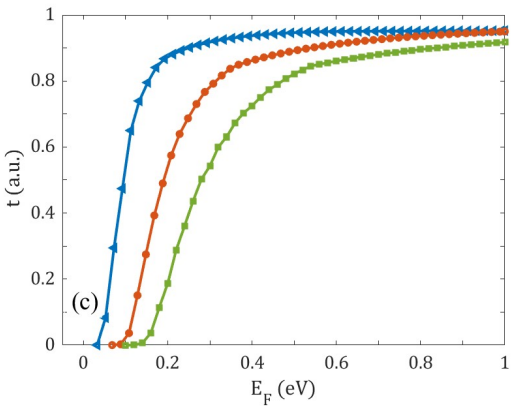

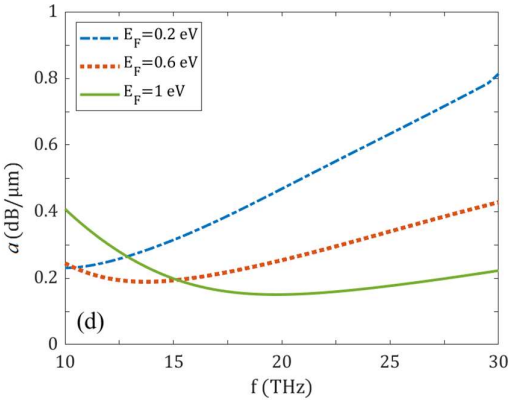

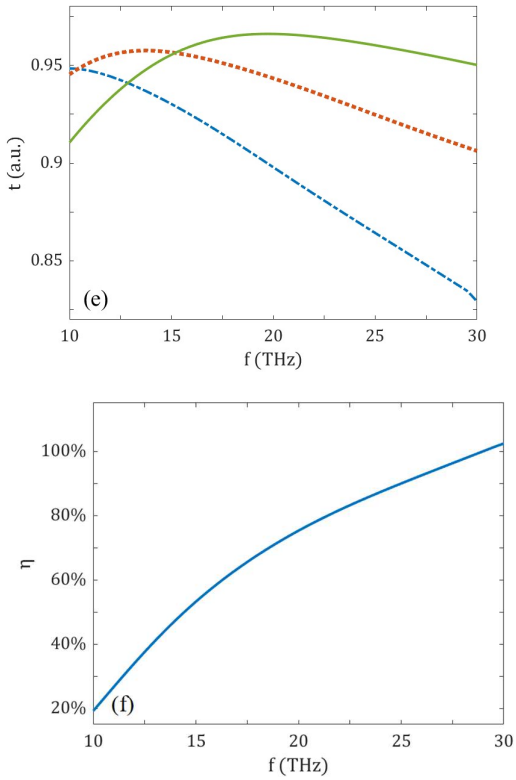

Figure 7. (a) The dependence of V_g on E_F, (b) and (c) the dependence of α (dB/μm) and the t coefficient on E_F in different frequencies, respectively. (d) and (e) the dependence of α (dB/μm) and t coefficient on f in different Fermi energies, respectively. (f) the modulation depth η on f.

4. Conclusions

In this research, the designed waveguide composed of dual semi-cylinder Germanium substrates has been exhibited for extremely efficacious broadband SPPs propagation and modulation in the MIR range. Because of the matchless waveguide configuration, greatly augmented electromagnetic wave interaction with graphene and subwavelength SPPs confinement can be attained. It is found that the SPPs mode has a longer propagation length (10.67-28.92 μm) in the MIR frequency range 10-30 THz with the Fermi energy of 1.0 eV. Also, it can be seen that the SPPs mode has a lesser normalized mode area ($\sim 10^{-4}$) in the MIR and the frequency range of 10-30 THz with the Fermi energy of 1.0 eV and radius R > 450 nm. By controlling the graphene Fermi energy from 0.2-1.0 eV, we have illustrated broadband modulation of MIR guided wave with a modulation depth larger than 20 % in the frequency range of 10-30 THz and a peak of approximately100 % at f > 28.75 THz. The designed waveguide proposes a prospective approach for superlative broadband MIR SPPs propagation and modulation, which may be utilized in different high-efficiency MIR devices.

References

[1] J. Xu, Z. Ren, B. Dong, X. Liu, C. Wang, Y. Tian and C Lee, "Nanometer-Scale Heterogeneous Interfacial Sapphire Wafer Bonding for Enabling Plasmonic-Enhanced Nanofluidic Mid-Infrared Spectroscopy." ACS Nano, **14** (2020) 12159.

[2] B. Fang et al., "Bidirectional mid-infrared communications between two identical macroscopic graphene fibers." nature communications, **11** (2020) 6368.

[3] A. Tittl et al., "A Switchable Mid-Infrared Plasmonic Perfect Absorber with Multispectral Thermal Imaging Capability." Advanced Materials, **27** (2015) 4597.

[4] J. Zhang et al., "Fano-Resonance in Hybrid Metal-Graphene Metamaterial and Its Application as Mid-Infrared Plasmonic Sensor." Micromachines, **11** (2020) 268.

[5] L. Ye, K. Sui, Y. Liu, M. Zhang and Q. Liu, "Graphene-based hybrid plasmonic waveguide for highly efficient broadband mid-infrared propagation and modulation." Optics Express, **26** (2018) 15935.

[6] M. R. Jafari and M. Omidi, "The effect of quantum ring size on shifting the absorption coefficient from infrared region to ultraviolet region." Applied Physics A, **125** (2019) 1.

[7] M. R. Jafari and B. Bahrami, "Emission properties of porphyrin compounds in new polymeric PS: CBP host." Applied Physics A, **119** (2015) 1491.

[8] D. K. Gramotnev and S. I. Bozhevolnyi, "Plasmonics beyond the diffraction limit." Nature Photonics, **4** (2010) 83.

[9] E. Ozbay, "Plasmonics: Merging photonics and electronics at nanoscale dimensions." Science, **311** (2006) 189.

[10] M. R. Jafari and F. Ebrahimi, "Plasmonic Thermal Conductance of Stack of Metallic Nanorings." Journal of Sciences Islamic Republic of Iran, **21** (2010) 279.

[11] M. Farhadi, M. Jafari and M. Shahmansouri, "Effective mass dependence of the gyrotropic nihility in a BaM/6H-SiC multilayer structure." Applied Physics A, **126** (2020) 1.

[12] N. Ranjkesh, M. Basha, A. Taeb, A. Zandieh, S. Gigoyan and S. Safavi-Naeini, "Silicon-on-glass dielectric waveguide—Part I: For millimeter-wave integrated circuits." IEEE Transactions on THz Science and Technology, **5** (2015) 268.

[13] T. S. Saini, A. Kumar and R. K. Sinha, "Broadband Mid-Infrared Supercontinuum Spectra Spanning 2-15 μm Using As_2Se_3 Chalcogenide Glass Triangular-Core Graded-Index Photonic Crystal Fiber." Journal of Lightwave Technology, **33** (2015) 3914.

[14] C. Yang, Q. Wu, J. Xu, K. A. Nelson and C. A. Werley, "Experimental and theoretical analysis of THz frequency, direction-dependent, phonon polariton modes in a subwavelength, anisotropic slab waveguide." Optics Express, **18** (2010) 26351.

[15] R. Zia, J. A. Schuller, A. Chandran and M. L. Brongersma, "Plasmonics: the next chip-scale technology." Materials Today, **9** (2006) 20.

[16] M. R. Jafari, F. Ebrahimi and M. Nooshirvani, "Subwavelength electromagnetic energy transport by stack of metallic nanorings." Journal of Applied Physics, **108** (2010) 054313.

[17] C. L. Smith, N. Stenger, A. Kristensen, N. A. Mortensen and S. I. Bozhevolnyi, "Gap and channeled plasmons in tapered grooves: a review." Nanoscale, **7** (2015) 9355.

[18] R. F. Oulton, V. J. Sorger, D. A. Genov, D. F. P. Pile and X. Zhang, "A hybrid plasmonic waveguide for subwavelength confinement and long-range propagation." Nature Photonics, **2** (2008) 496.

[19] Z. Zhang and J. Wang, "Long-range hybrid wedge plasmonic waveguide." Scientific Reports, **4** (2014) 6870.

[20] Y. Gao, G. Ren, B. Zhu, J. Wang and S. Jian, "Single-mode graphene-coated nanowire plasmonic waveguide." Optics Letters, **39** (2014) 5909.

[21] A. K. Geim, "Graphene: status and prospects." Science, **324** (2009) 1530.

[22] A. N. Grigorenko, M. Polini and K. S. Novoselov, "Graphene plasmonics." Nature Photonics, **6** (2012) 749.

[23] M. Esmaeili, M. R. Jafari, M. Sanaeepur, "Negative differential resistance in nanoscale heterostructures based on zigzag graphene nanoribbons anti-symmetrically decorated with BN." Superlattices and Microstructures, **145** (2020) 106584.

[24] A. Asadi, M. R. Jafari, M. Shahmansouri, "Simulation optimized design of graphene-based hybrid plasmonic waveguide." Indian Journal of Physics, Published: 30 January (2023).

[25] X. He, T. Ning, L. Pei, J. Zheng, J. Li and J. Wang, "Deep subwavelength graphene-dielectric hybrid plasmonic waveguide for compact photonic integration." Results in Physics, **21** (2021) 103834.

[26] V. W. Brar, M. S. Jang, M. Sherrott, J. J. Lopez and H. A. Atwater, "Highly confined tunable mid-infrared plasmonics in graphene nanoresonators." Nano Letters, **13**, (2013) 2541.

[27] M. Shahmansouri, B. Farokhi and R. Aboltaman, "Exchange interaction effects on low frequency surface waves in a quantum plasma slab." Physics of Plasmas, **24** (2017) 054505.

[28] R. Aboltaman and M. Shahmansouri, "Boundary graphene layer effect on surface plasmon oscillations in a quantum plasma half-space." Communications in Theoretical Physics, **72** (2020) 045501.

[29] L. Jiang, C. Yuan, Z. Li, J. Su, Z. Yi, W. Yao, P. Wu, Z. Liu, S. Cheng and M. Pan, "Multi-band and high-sensitivity perfect absorber based on monolayer graphene metamaterial." Diamond & Related Materials, **111** (2020) 108227.

[30] F. Jabbarzadeh and A. Habibzadeh-Sharif, "High performance dielectric loaded graphene plasmonic waveguide for refractive index sensing." Optics Communications, 479 (2021) 126419.

[31] Y. Sharma, R. R. Ghosh, V. Sapra, V. Jalal, K. Ahmed and A. Dhawan, "Plasmonic switches based on arrays of plasmonic nanostructures surrounded by VO_2 thin films." Quantum Sensing and Nano Electronics and Photonics XVI, **10926** (2019) 109262S.

[32] D. Rodrigo, O. Limaj, D. Janner, D. Etezadi, F. J. García de Abajo, V. Pruneri and H. Altug, "Mid-infrared plasmonic biosensing with graphene." Science, **349** (2015) 165.

[33] L. Luo, K. Wang, C. Ge, K. Guo, F. Shen, Z. Yin and Z. Guo, "Actively controllable terahertz switches with graphene-based nongroove gratings." Photonics Research, **5** (2017) 604.

[34] M. Liu, X. Yin and X. Zhang, "Double-layer graphene optical modulator." Nano Letters, **12** (2012) 1482.

[35] A. Asadi, M. R. Jafari, M. Shahmansouri, "Characteristics of a Symmetric Mid-infrared Graphene Dielectric Hybrid Plasmonic Waveguide with Ultra-

.

deep Subwavelength Confinement." Plasmonics, **17** (2022) 1819.

[36] D. Teng, Y. Wang, T. Xu, H. Wang, Q. Shao and Y. Tang, "Symmetric Graphene Dielectric Nanowaveguides as Ultra-Compact Photonic Structures," Nanomaterials **11** (2021) 1281.

[37] M. Shahmansouri and M. Mahmodi-Moghadam, "Quantum electrostatic surface waves in a hybrid plasma waveguide: Effect of nano-sized slab." Physics of Plasmas, **24** (2017) 102107.

[38] M. Mahmodi-Moghadam and M. Shahmansouri, "Theoretical study of surface waves in a magnetized conductor-gap-dielectric nano-structure." Physica Scripta, **95** (2020) 085606.

[39] Y. Zhao et al., "Enhanced SERS Stability of R6G Molecules with Monolayer Graphene." The Journal of Physical Chemistry C, **118** (2014) 11827.

[40] P. Wang, O. Liang, W. Zhang, T. Schroeder and Y. H. Xie, "Ultra-Sensitive Graphene-Plasmonic Hybrid Platform for Label-Free Detection." Advanced Materials, **25** (2013) 4918.

[41] T. Tite et al., "Graphene-based textured surface by pulsed laser deposition as a robust platform for surface enhanced Raman scattering applications." Applied Physics Letters, **104** (2014) 41912.

[42] Y. Hajati, Z. Zanbouri and M. Sabaeian, "Low-loss and high-performance mid-infrared plasmon-phonon in graphene-hexagonal boron nitride waveguide." Journal of the Optical Society of America B, **35** (2018) 446.

[43] G. W. Hanson, "Dyadic Green's functions for an anisotropic, non-local model of biased graphene." IEEE Transactions on Antennas Propagation, **56** (2008) 747.

[44] Q. Zhang, X. Li, M. M. Hossain, Y. Xue, J. Zhang, J. Song, J. Liu, M. D. Turner, S. Fan, Q. Bao, and M. Gu, "Graphene surface plasmons at the near-infrared optical regime." Scientific Reports, **4** (2014) 6559.

[45] W. Xu, Z. H. Zhu, K. Liu, J. F. Zhang, X. D. Yuan, Q. S. Lu, and S. Q. Qin, "Toward integrated electrically controllable directional coupling based on dielectric loaded graphene plasmonic waveguide." Optics Letters, **40** (2015) 1603.

[46] J. S. Gómez-Díaz, M. Esquius-Morote, and J. Perruisseau-Carrier, "Plane wave excitation-detection of nonresonant plasmons along finite-width graphene strips." Optics Express, **21** (2013) 24856.

[47] K. I. Bolotin, K. J. Sikes, Z. Jiang, M. Klima, G. Fudenberg, J. Hone, and H. L. Stormer, "Ultrahigh electron mobility in suspended graphene." Solid State Communications, **146** (2008) 351.

[48] W. Gao, J. Shu, C. Qiu, and Q. Xu, "Excitation of plasmonic waves in graphene by guided-mode resonances." ACS Nano, **6** (2012) 7806.

[49] C. R. Dean, A. F. Young, I. Meric, C. Lee, L. Wang, S. Sorgenfrei, K. Watanabe, T. Taniguchi, P. Kim, K. L. Shepard, and J. Hone, "Boron nitride substrates for high-quality graphene electronics." Nature Nanotechnology, **5** (2010) 722.

[50] X. Chen, et al., "A Broadband Optical Modulator Based on a Graphene Hybrid Plasmonic Waveguide." Journal of Lightwave Technology, 34 (2016) 4948.

[51] Y. Zhang, S. Qiao, S. Liang, Z. Wu, Z. Yang, Z. Feng, H. Sun, Y. Zhou, L. Sun, Z. Chen, X. Zou, B. Zhang, J. Hu, S. Li, Q. Chen, L. Li, G. Xu, Y. Zhao, and S. Liu, "Gbps terahertz external modulator based on a composite metamaterial with a double-channel heterostructure." Nano Letters, **15** (2015) 3501.